

1 **Detection of delay in post-monsoon agricultural burning across** 2 **Punjab, India: potential drivers and consequences for air quality**

3 Tianjia Liu^{1*}, Loretta J. Mickley^{2*}, Ritesh Gautam³, Manoj K. Singh⁴, Ruth S. DeFries⁵,
4 and Miriam E. Marlier⁶

5 ¹Department of Earth and Planetary Sciences, Harvard University, Cambridge, MA, 02138, USA

6 ²School of Engineering and Applied Sciences, Harvard University, Cambridge, MA, 02138,
7 USA

8 ³Environmental Defense Fund, Washington, D.C., 20009, USA

9 ⁴University of Petroleum and Energy Studies, Dehradun, Uttarakhand, India

10 ⁵Department of Ecology, Evolution, and Environmental Biology, Columbia University, New
11 York, NY, 10027, USA

12 ⁶RAND Corporation, Santa Monica, CA, 90401, USA

13

14 *Correspondence to: Tianjia Liu (tianjialiu@g.harvard.edu), Loretta Mickley
15 (mickley@fas.harvard.edu)

16 **Abstract**

17 Since the Green Revolution in the mid-1960s, a widespread transition to a rice-wheat
18 rotation in the Indian state of Punjab has led to steady increases in crop yield and production.
19 After harvest of the summer monsoon rice crop, the burning of excess crop residue in Punjab
20 from October to November allows for rapid preparation of fields for sowing of the winter wheat
21 crop. Here we use daily satellite remote sensing data to show that the timing of peak post-
22 monsoon fire activity in Punjab and regional aerosol optical depth (AOD) has shifted later by
23 approximately two weeks in Punjab from 2003-2016. This shift is consistent with delays of 11-
24 15 days in the timing of maximum greenness of the monsoon crop and smaller delays of 4-6 days
25 in the timing of minimum greenness during the monsoon-to-winter crop transition period. The
26 resulting compression of the harvest-to-sowing period coincides with a 40% increase in total
27 burning and ~50% increase in regional AOD. Potential drivers of these trends include
28 agricultural intensification and a recent groundwater policy that delays sowing of the monsoon
29 crop. The delay and amplification of burning into the late post-monsoon season suggest greater
30 air quality degradation and public health consequences across the densely-populated Indo-
31 Gangetic Plain.

32 **1. Introduction**

33 Rapid increases in mechanized harvesting in the Indo-Gangetic Plain (IGP) since the
34 mid-1980s, together with steady increases in crop production, have led many farmers to burn the
35 abundant residue left behind by this practice (Badarinath *et al* 2006). Such burning is a quick,
36 cheap, and efficient method to ready the fields for the next crop. However, the smoke from post-
37 monsoon crop residue burning, primarily during October to November, amplifies severe haze
38 events in the region (Kaskaoutis *et al* 2014, Bikkina *et al* 2019), such as that observed in early
39 November 2016 (Cusworth *et al* 2018). Of particular concern is the observed increase in aerosol
40 loading associated with an increasing trend in post-monsoon burned area and shift toward a later

41 peak in post-monsoon fires in northwestern India (Thumaty *et al* 2015, Jethva *et al* 2018, Liu *et*
42 *al* 2019). Here we use daily satellite remote sensing data to better quantify the temporal shift
43 toward later burning in the state of Punjab, the “breadbasket” of India. Such a shift would have
44 implications for air quality, since peak burning is more likely to coincide with meteorological
45 conditions that are favorable in amplifying persistent haze.

46 Agricultural intensification of rice and wheat in India has led to over two-fold and three-
47 fold increases, respectively, in crop yield since the Green Revolution in the 1960s; consequently,
48 rice and wheat have become the mainstays of domestic food production (Mukherjee *et al* 2014).
49 As the largest single grain stockholder in the country, the Indian government subsidizes
50 production of these two crops through guaranteed purchase prices, and the resulting stocks form
51 the basis of a federal food distribution program (Swaminathan 2000, Dreze and Khera 2015). In
52 addition to its importance to Indian food security, agriculture is the primary source of income for
53 58% of Indian rural households, underscoring the critical nature of the timing and robustness of
54 the double-crop cycle on the rural economy (NSSO 2014). Punjab, an agricultural state in
55 northwestern India, contributes more than one-fifth of rice and one-third of wheat to the central
56 grain pool in India, and thus generates large amounts of crop residue annually. Since the mid-to-
57 late 1980s, farmers have increasingly used mechanized harvesting methods in preference to
58 sickle-based manual harvesting in order to reduce labor costs and save time (Badarinath *et al*
59 2006, Kumar *et al* 2015). The use of combine harvesters, however, leaves behind abundant loose
60 and root-bound residues that are difficult to remove and thus often burned post-harvest to prepare
61 for timely sowing of the next crop (Kumar *et al* 2015). The burning allows for quick disposal of
62 crop residues and shortens the harvest-to-sowing transition from the *kharif* (monsoon crop) to
63 *rabi* (winter crop) season. A quicker transition between crops also allows for earlier sowing of
64 wheat during post-monsoon to avoid springtime heat (Lobell *et al* 2013).

65 However, the burning of post-monsoon rice residue can severely degrade air quality
66 downwind of the agricultural fires over the IGP (Badarinath *et al* 2006, Kaskaoutis *et al* 2014,
67 Liu *et al* 2018, Cusworth *et al* 2018, Jethva *et al* 2018, Sarkar *et al* 2018). In particular, smoke
68 from rice residue burning in October and November may account for more than 40% of fine
69 particulate matter (PM_{2.5}) concentrations in the Delhi National Capital Region (Cusworth *et al*
70 2018, Bikkina *et al* 2019), which already experiences intense urban pollution from local and
71 other regional sources (Amann *et al* 2017). A temporal shift in fire activity to later in the year
72 could exacerbate air quality degradation since late autumn-to-winter meteorology in the IGP
73 favors smog formation due to weak winds, frequent temperature inversion, and a shallow
74 boundary layer (Choudhury *et al* 2007, Saraf *et al* 2010, Liu *et al* 2018).

75 Observations from the Moderate Resolution Imaging Spectroradiometer (MODIS),
76 aboard NASA’s Terra and Aqua satellites, have been extensively used to investigate fire activity,
77 crop yields, production, and phenology, and land use change detection. While MODIS multi-day
78 composites (8-day, 16-day) are typically used and require less computational power to pre-
79 process and analyze, they are insufficient for capturing and resolving rapid changes in crop
80 phenology (Zhao *et al* 2009). Here we use daily active fire and surface reflectance data from
81 MODIS to investigate trends in crop phenology and agricultural fire activity in Punjab. While the
82 moderate spatial resolution of MODIS likely leads to large underestimates in total post-monsoon
83 agricultural fire activity in northwestern India (Liu *et al* 2019), here we aim to quantify linear
84 trends using the relative temporal distribution, which is impacted less by spatial resolution. We
85 also determine whether the seasonal cycle of monsoon to post-monsoon vegetation greenness

86 reveals similar temporal shifts. We conclude with a discussion of the potential drivers of these
87 interannual changes and an analysis of the consequences for regional air quality.

88 **2. Data and Methods**

89 *2.1 Study region*

90 The IGP is home to over 700 million people ([appendix S1.4](#)), many of whom rely on
91 productivity of the croplands across northern India and parts of Pakistan, Nepal, and Bangladesh
92 for livelihood and food security. Relative to other double-cropped states in northern India, such
93 as Haryana, Uttar Pradesh, and Bihar, Punjab has the highest rice-wheat productivity (Kumar *et al*
94 *2015*) and is spatially more homogenous in terms of fire intensity ([Figure 1a](#)), rice-wheat
95 yields, and topography (Azzari *et al* 2017). Here we focus on Punjab during the post-monsoon
96 rice residue burning season (October to November), when fields are prepared for winter wheat
97 sowing. To a lesser degree, we examine the pre-monsoon wheat residue burning season (April-
98 May), when fields are prepared for monsoon rice sowing ([Figure 1b](#)).

99 *2.2 Active fires and vegetation indices*

100 For analysis of fire activity, we sum daily 1-km maximum of Fire Radiative Power
101 (FRP), a proxy for fire intensity, derived from MODIS/Terra and Aqua (MOD14A1/MYD14A1,
102 Collection 6; Giglio *et al* 2016). For analysis of vegetation greenness, we use daily 500-m
103 MODIS/Terra surface reflectance (MOD09GA, Collection 6) to derive two vegetation indices,
104 the Normalized Difference Vegetation Index (NDVI) and Normalized Burn Ratio (NBR):

$$105 \quad \text{NDVI} = \frac{\rho_2 - \rho_1}{\rho_2 + \rho_1} \quad (1)$$

$$106 \quad \text{NBR} = \frac{\rho_2 - \rho_7}{\rho_2 + \rho_7} \quad (2)$$

107 where ρ_i is the surface reflectance of MODIS band i . The wavelength range of the bands is as
108 follows: 620-670 nm for band 1 (red), 841-876 nm for band 2 (near infrared), and 2105-2155 nm
109 for band 7 (shortwave infrared). [Section 2.3.2](#) further describes the vegetation indices, and
110 [appendix S1](#) describes in detail the MODIS fire and surface reflectance datasets used in this
111 study.

112 *2.3 Statistical analysis*

113 We estimate linear trends with residuals bootstrapping. Unlike the linear regression t-test,
114 which assumes that the residuals are normally distributed, bootstrapping preserves and resamples
115 from the sample residuals distribution. To obtain a sample distribution, 1000 iterations are
116 performed in which residuals are randomly sampled with replacement for each iteration and the
117 dependent variable y re-fit using linear regression.

118 *2.3.1 Characterizing the temporal progression of agricultural fires*

119 We characterize the progression of the pre-monsoon and post-monsoon burning seasons,
120 defined in [Section S2.1](#), of each year in order to assess interannual temporal trends. Following

121 Zhang *et al* (2014), we estimate the start, midpoint, and end of the pre-monsoon and post-
122 monsoon burning seasons for each year. First, let $X = \{x_t \mid x_1, x_2, x_3 \dots x_n\}$ denote the daily time
123 series of a fire metric, such as FRP, during a given burning season lasting n number of days. We
124 define the pre-monsoon (April 1-May 31) and post-monsoon (September 20-November 30)
125 burning seasons with broad windows in order to capture all possible seasonal fire activity. We
126 can then define a sequence of partial sums, $Y = \{y_k \mid y_1, y_2, y_3 \dots y_n\}$, in which $y_k = \sum_{t=1}^k x_t$.
127 We normalize y_k by y_n , or the sum of FRP during the entire burning season. We then
128 approximate k_β , or the first day when normalized Y has surpassed breakpoint β :

$$129 \quad k_\beta = \arg \min_k \left[\left(\frac{y_k}{y_n} - \beta \right) > 0 \right] \quad (3)$$

130 As in Zhang *et al* (2014), we define arbitrary breakpoints, $\beta = 0.1, 0.5$, and 0.9 , to represent the
131 start ($k_{\beta=0.1}$ or k_{start}), midpoint ($k_{\beta=0.5}$ or $k_{midpoint}$), and end ($k_{\beta=0.9}$ or k_{end}), respectively, of
132 the burning season. However, the value $k_{midpoint}(FRP)$ may not correspond to the day of peak
133 burning, $k_{peak}(FRP)$. To estimate $k_{peak}(FRP)$, we fit Gaussian density curves to daily FRP,
134 thus smoothing potential noise in FRP due to inconsistencies in observing area caused by cloud
135 and haze cover:

$$136 \quad g(t) = \gamma \cdot e^{-0.5 \left[\frac{(t-\mu)}{\sigma} \right]^2} \quad (4)$$

137 where $g(t)$ is the Gaussian function to be optimized, t is days of the burning season expressed as
138 1 to n total days, μ is the mean of t , σ is the standard deviation of t , and γ is an arbitrary scaling
139 parameter. We then use the *optim* function from the R *stats* package to minimize nonlinear least
140 squares of $g(t)$ and fractional daily FRP and to estimate the μ , σ , and γ parameters that yield the
141 optimal Gaussian fit. As first guesses of the three parameters for the *optim* function, we use
142 $k_{midpoint}(FRP)$ as μ , 7 as σ , and 1 as γ .

143 2.3.2 Tracking crop phenology with NDVI and NBR

144 NDVI is widely used to characterize the cycling in vegetation growth, land cover change,
145 and crop productivity (Yengoh *et al* 2015, Justice *et al* 1985). NBR, while typically used in
146 burned area and burn severity classification (Key and Benson 2006), is analogous to NDVI,
147 which relies on the visible red reflectance instead of the shortwave infrared (SWIR) reflectance.
148 A major advantage of NBR is that compared to visible wavelengths, SWIR wavelengths can
149 better discriminate between vegetation and bare soil (Chen *et al* 2005, Asner and Lobell 2000)
150 and are less susceptible to atmospheric interference from smoke aerosols and thin clouds (Roy *et al*
151 1999, Eva and Lambin 1998, Avery and Berlin 1992). Here we use NBR as a complement to
152 NDVI to track crop phenology with variations in vegetation greenness.

153 We estimate the timing of crop maturation, or maximum greenness, during the monsoon
154 growing season with both the daily median NDVI and NBR time series. Assuming that the
155 seasonal progression in the crop cycle is similar across years, the timing of peak greenness in the
156 growing season diagnoses the timing of the overall growing season. However, cloud and aerosol
157 contamination can introduce noise in satellite retrievals (Platnick *et al* 2003). To estimate the
158 timing of the maximum monsoon greenness with the noisy daily time series, we apply weighted
159 cubic splines smoothing with bootstrapping on time steps within a defined window that straddles

160 the day of monsoon peak greenness. Cubic splines smoothing stitches together piecewise third-
161 order polynomial interpolation between “knots,” or selected experimental points, and has been
162 used extensively for crop phenology applications (Jain *et al* 2013, Mondal *et al* 2014, 2015, Jain
163 *et al* 2017). We apply weights to the NDVI and NBR time series using the daily fraction of
164 “usable” pixels, or those uncontaminated by clouds or thick haze (hereafter referred to as usable
165 fraction) in the study area. This weighting follows from our greater confidence in daily median
166 NDVI and NBR on clearer days versus cloudier and/or hazier days. Prior to bootstrapping, we
167 make initial guesses of the four local maxima and minima: monsoon and winter peak greenness
168 and pre-monsoon and post-monsoon trough greenness. We use these initial guesses to center a
169 window of 300 days. Using a smoothing parameter of 0.75, we smooth the vegetation index time
170 series with weighted cubic splines within the defined window and estimate the bootstrapped
171 mean timing of maximum NDVI or NBR for each year. We repeat this process to estimate the
172 earliest date when fields are ready to sow the winter crop, or trough greenness, during the post-
173 monsoon transition period.

174 *2.3.3 Regional aerosol optical depth exceedances*

175 To quantify enhancements in regional air quality degradation during the post-monsoon
176 burning season, we use MODIS/Terra Deep Blue retrievals of aerosol optical depth (AOD) over
177 Punjab, Haryana, Delhi, and western Uttar Pradesh (i.e., encompassing both the aerosol source
178 and downwind transport regions of the IGP; [appendix S1.3](#)). In order to minimize the
179 contribution of background AOD, we analyze regionally averaged AOD “exceedances” – that is,
180 the daily spatial mean of AOD above the mean AOD + 1σ for each pixel and season across
181 Punjab, Haryana, Delhi, and western Uttar Pradesh at 0.25° resolution. We analyze these daily
182 mean AOD exceedances within the $k_{start}(FRP)$ and $k_{end}(FRP)$ window to isolate the effect of
183 agricultural burning. To estimate the timing of peak AOD exceedances, or $k_{peak}(AOD)$, we
184 apply Gaussian density curve optimization to values within this window expanded by four
185 weeks. Such expansion ensures that the optimization is not thrown off by high AOD days
186 isolated at the beginning or end of the season.

187 **3. Results**

188 *3.1 Trends in seasonal agricultural fire activity*

189 The bimodal distribution of peak agricultural fire activity in both pre-monsoon and post-
190 monsoon periods is limited to northwestern India, primarily in Punjab, as well as northern
191 Haryana ([Figures 1, S1](#)). Generally, 80% of post-monsoon fires in Punjab are set within an
192 approximate three-week window (23 ± 3 days) from mid-October to early November. We
193 estimate that the timing of peak post-monsoon fire intensity has shifted later in Punjab by 1.16
194 days yr^{-1} (95% CI: [0.81, 1.49]), statistically significant at the 95% confidence interval (CI),
195 indicating that the burning of rice residue has shifted later by over two weeks from 2003-2016
196 ([Figure 2, Table S2](#)). These findings are corroborated by similar temporal and magnitude shifts
197 in GFEDv4s fire emissions and MODIS fire counts and burned area ([Table S3](#)). In contrast, we
198 generally find no such statistically significant delays in the pre-monsoon burning season in
199 Punjab ([Table S2](#)).

200 Spatially, the post-monsoon temporal shift is larger in magnitude in districts in western
201 Punjab than in eastern Punjab ([Figure S3](#)). Moreover, the 14-year trends in total fire intensity for

202 each 3-day block within this window signal a shift in the peak burning period, with decreasing
203 FRP in mid-to-late October and increasing FRP in early November (Figure 2). The magnitude of
204 peak post-monsoon fire activity, indicated by the 99th percentile of 3-day block sums of FRP,
205 has doubled over the 14-year period, an increase that may be partly attributed to some
206 homogenization in the timing of burning across districts.

207 3.2 Trends in vegetation greenness from monsoon to post-monsoon

208 We also examine whether vegetation greenness in Punjab show similar shifts during the
209 monsoon growing season and post-monsoon harvest-to-sowing transition period. Whereas the
210 timing of minimum NBR and NDVI occurs after near-completion of post-monsoon burning in
211 mid-to-late November, the temporal maximum of these vegetation indices occurs near the end of
212 the monsoon around late August or early September (Figure 1b), indicating crop maturation. In
213 Punjab, the timing of maximum NDVI and NBR shows an overall delay of 11-15 days, with a
214 large, abrupt shift of 7-9 days around 2008-09 (Figure 3a-b). Concurrently, there is an evident
215 increasing trend in maximum monsoon NBR (0.06 decade^{-1} , 95% CI: [0.04, 0.08]) and NDVI
216 (0.07 decade^{-1} , 95% CI: [0.05, 0.09]), consistent with steady increases in annual total *kharif* rice
217 production in Punjab of 0.13 Tg yr^{-1} (95% CI: [0.09, 0.17]) (Figures 3b, S4, Table S5). Such
218 increases in peak NBR and NDVI also suggest greater quantities of crop residue, which may lead
219 to amplified fire intensity and emissions. In contrast to the shift in maximum NBR and NDVI,
220 we find a smaller delay of 4-6 days in the timing of the minimum values of these indices during
221 post-monsoon (Figure 3c-d, Table S5), indicating that the shift in the monsoon growing season is
222 greater than the corresponding shift in the timing of the earliest date when fields are ready for
223 winter wheat sowing. In addition, we find that the duration from the start of the burning season
224 to trough post-monsoon greenness has decreased by $0.71 \text{ days yr}^{-1}$ (95% CI: [-1.03, -0.39]),
225 providing evidence for a shortened harvest-to-sowing period (Figure S5). Taken together, our
226 results suggest that the temporal shifts in post-monsoon burning are likely associated with later
227 sowing and harvesting of the monsoon crop.

228 3.2.1 The utility of NBR as a vegetation index

229 We have so far considered NBR and NDVI as complementary vegetation indices. Here
230 we further demonstrate the utility of NBR for tracking crop phenology, particularly in resolving
231 the troughs of the crop cycle. First, NBR is more sensitive than NDVI to the progression in the
232 post-monsoon burning season. The mean drawdown in NBR per unit increase in β is ~30%
233 higher in magnitude than that of NDVI for Punjab (Figure S6). This suggests that NDVI may be
234 more susceptible to saturation at low values of vegetation greenness than NBR during the post-
235 harvest and post-burning period. The weaker detrended correlations ($r = 0.23 \pm 0.39$) between
236 the two vegetation indices during transition months between the *kharif* and *rabi* seasons (May,
237 June, October, and November) compared to other months ($r = 0.88 \pm 0.12$) support the notion
238 that NDVI more poorly resolves and tends to “flatten” the troughs of the double-crop cycle curve
239 (Figure S7). Moreover, the monthly distributions of detrended $r(\text{NDVI}, \text{NBR})$ values closely
240 follow variations in greenness in the double-crop cycle, with greater correlation during seasons
241 of crop growth. This pattern of correlation suggests that the performance of NDVI depends on
242 the level of greenness in-field and that NDVI values at or near-minimum greenness should be
243 interpreted with caution.

244 3.3 Trends in post-monsoon regional aerosol optical depth

245 To quantify the consequences of the delays in post-monsoon agricultural fire activity for
246 regional air quality, we assess AOD exceedances during the main burning period bounded by
247 $k_{start}(FRP)$ and $k_{end}(FRP)$. Within this window, post-monsoon AOD exceedances have
248 increased by 54% from 2003-2016, likely associated with the reported upward trend in fire
249 intensity (Figure 4). Similar to the magnitude of the delay in $k_{peak}(FRP)$, the timing of the peak
250 in AOD, $k_{peak}(AOD)$, has shifted by 0.8 days yr^{-1} (95% CI: [0.46, 1.1]), or ~11 days during the
251 14-year period. The delay and increase in post-monsoon agricultural fire activity appear to drive
252 the coherent shifting pattern in heavy aerosol loading episodes (higher AOD exceedances),
253 notably observed in early November after 2008, despite the variability in AOD impacted by
254 meteorology and other pollution sources, such as fireworks during the Diwali festival. Diwali
255 lasts several days, and its timing is highly variable from year to year (October-November),
256 following the lunar calendar.

257 4. Discussion

258 4.1 Implications of delays in post-monsoon fire activity

259 We find that the peak fire intensity of the post-monsoon burning season in Punjab has
260 shifted later in time by over two weeks from 2003 to 2016, with a 40% increase in overall fire
261 intensity. This delay is gradual, likely influenced by steady increases in crop production and
262 mechanization, which yield higher amounts of excess crop residue. We hypothesize that a
263 shortened harvest-to-sowing turnaround time after *kharif* rice harvests has amplified this increase
264 by making it difficult for farmers to prepare fields for timely sowing of *rabi* wheat. The optimal
265 time to sow wheat in Punjab is late October to early November (Balwinder-Singh *et al* 2016, Liu
266 *et al* 2019), yet co-occurring post-monsoon fires indicate that fields are often not ready at this
267 time, particularly in recent years. Since fire is a quick and cheap method to remove the leftover
268 residue generated by combine harvesters, farmers may have even greater incentive to burn crop
269 residue, especially if harvests are delayed past the optimal date to sow wheat. Consistent with
270 this hypothesis, we find that high fire intensity days preferentially occur during the latter half of
271 the fire season, when the optimal window for sowing is shrinking. As post-monsoon fires
272 increase in response to mechanization and pressures to sow on time, the burning season
273 gradually trends later, further compressing the harvest-to-sowing window and increasing fire
274 intensity rates. As a result, winter wheat sow dates across the region will likely homogenize,
275 collapsing around a small optimal window to mitigate crop losses from increasing temperatures
276 from February to March (Lobell *et al* 2012).

277 Additionally, we estimate a ~50% increase in regional AOD exceedances and ~11-day
278 delay in the timing of peak AOD within the post-monsoon burning period from 2003-2016.
279 Delays in the post-monsoon burning season also suggest that high fire activity periods may
280 increasingly coincide with late-autumn/winter meteorological conditions that favor severe
281 fog/smog and haze events across the IGP (Dey 2018). Dense fog formation peaks in winter
282 (December to January) over the IGP (Dey 2018, Gautam and Singh 2018, Ghude *et al* 2017), but
283 in recent years there appears to be an increasing tendency in dense fog episodes observed earlier
284 in November, coinciding with the buildup of intense smoke associated with crop residue burning
285 activity (Figure S8). Aside from increasing exposure to high regional particulate matter

286 concentrations both locally and in urban centers downwind, crop residue burning depletes soil
287 moisture and decreases roadside visibility (Kumar *et al* 2015, Badarinath *et al* 2006, Sidhu *et al*
288 2015, Sinha *et al* 2015). In spite of bans, such burning continues to persist and gain traction
289 (Tallis *et al* 2017). New technology that simultaneously reuses crop residue as mulch cover and
290 incorporates seeds into the bare soil has been tested as an alternative to slash-and-burn methods
291 of managing crop residue (Sidhu *et al* 2015, Tallis *et al* 2017).

292 *4.2 Potential drivers of delays in the rice-wheat rotation*

293 Delays in the post-monsoon burning season are consistent with such shifts in the timing
294 of monsoon peak greenness (11-15 days) and post-monsoon trough greenness (4-6 days), though
295 of lesser magnitude. Unlike the steady shifts seen in post-monsoon burning, an abrupt delay of
296 roughly one week occurring around 2008-09 dominates the overall delay in the timing of
297 monsoon peak greenness, with relatively little change thereafter. Abrupt delays of similar
298 magnitude are also apparent in the timing of the start of the post-monsoon burning season. Here
299 we consider whether policy changes implemented around this time may have contributed toward
300 these abrupt shifts. In 2009, in order to counteract severe groundwater depletion driven by low
301 monsoon rainfall and widespread agricultural intensification, the Government of Punjab enacted
302 the "Preservation of Sub-Soil Water Act" (ordinance in 2008), which prohibits sowing rice
303 nurseries before May 10 and transplanting the resulting rice seedlings to flooded paddies before
304 June 10 (Ramanathan *et al* 2005, Asoka *et al* 2017, Singh 2009, Tripathi *et al* 2016). The Act
305 delays the onset of water-intensive agricultural practices that would otherwise coincide with
306 warm temperatures and high pre-monsoon evapotranspiration rates, which lead to excessive
307 usage of the groundwater supply from tube wells and other reservoirs (Humphreys *et al* 2010).

308 Another policy that could be related to the shift is the 2008 all-India implementation of
309 the Mahatma Gandhi National Rural Employment Guarantee Act (MGNREGA), a measure that
310 provides a social security net to rural workers (Reddy *et al* 2014) and may have decreased the
311 seasonal migration of workers to Punjab and led to labor shortages there (Singh 2009). Such
312 shortages may have delayed the sowing of rice and incentivized use of combine harvesters,
313 which may in turn explain the increase in crop residue burning. However, the already widespread
314 transition to mechanized harvesting in Punjab, with diminishing dependence on manual labor,
315 suggests that MGNREGA may have had a smaller impact on the timing of harvest and burning.
316 Finally, variations in the timing of monsoon onset and withdrawal may be partly responsible for
317 the interannual variability in these observed shifts, such as the early monsoon onset and rice
318 maturation in 2013, but do not appear to drive the overall one-week delay in peak monsoon
319 greenness from the 2003-2007 to 2008-2016 time periods (Figure S9). It is important to note that
320 here we do not establish direct causality with the groundwater policy, MGNREGA, or monsoon
321 rainfall variability, but suggest a relationship that needs to be further explored in the field. Figure
322 S10 summarizes the potential drivers and implications of the delay in and amplification of post-
323 monsoon fire activity associated with double-crop cycle.

324 **5. Conclusion**

325 In summary, we show robust, statistically significant temporal shifts of over two weeks in
326 the timing of peak fire activity during the post-monsoon burning period in Punjab over a 14-year
327 period from 2003-2016, and smaller delays of 11-15 days in monsoon peak greenness and 4-6

328 days in post-monsoon trough greenness. We estimate the start, midpoint, and end of the burning
329 season by using the partial sums of FRP and the timing of peak FRP and regional AOD
330 exceedances by optimizing the Gaussian mean. We further demonstrate the viability and
331 applicability of using daily MODIS surface reflectance to characterize crop cycles and the utility
332 of NBR as a useful complement to NDVI for quantifying these vegetation changes. We
333 hypothesize that while the gradual delays in the post-monsoon burning season are likely linked to
334 agricultural intensification and increasing mechanization, the abrupt delay of one week around
335 2008-09 seen in the monsoon crop growing season appears to coincide with the state-wide
336 groundwater policy. The unintended consequences of these temporal shifts in the double-crop
337 cycle may be severe. First, a shortened harvest-to-sowing period may further encourage farmers
338 to burn crop residues in order to sow winter wheat on time. Second, the timing of peak crop
339 residue burning may increasingly coincide with winter meteorology that favors severe smog
340 events downwind across the IGP, where we diagnose a ~50% increase in AOD exceedances,
341 defined as the increment of AOD above the mean + 1σ , over 2003-2016. Alternative technology
342 that combines the co-benefits of incorporating wheat seeds with rice residue and eliminating the
343 need to burn residue, as well as switching to less water-intensive and stubble-producing crops,
344 may alleviate the double bind of having to conserve groundwater while reducing public health
345 exposure to smoke from post-monsoon fires.

346 **Data Availability**

347 All satellite-derived data used in this study are publicly available. MODIS-derived datasets can
348 be accessed through NASA Earthdata (<https://search.earthdata.nasa.gov/>) and Google Earth
349 Engine (Gorelick *et al* 2017) (<https://earthengine.google.com/>). The Global Fire Emissions
350 Dataset, version 4s, (GFEDv4s) and MODIS and VIIRS active fire geolocations are available
351 from GFED (<http://www.globalfiredata.org/>), University of Maryland
352 (<http://fuoco.geog.umd.edu/>), and NASA Fire Information for Resource Management System
353 (FIRMS) (<https://firms.modaps.eosdis.nasa.gov/>).

354 **Acknowledgements**

355 We thank Marena Lin and Peter Huybers for key contributions to early versions of this work and
356 Meghna Agarwala for helpful comments regarding this manuscript. This work was supported by
357 a National Science Foundation Graduate Research Fellowship awarded to T.L. (DGE1745303).

358 **References**

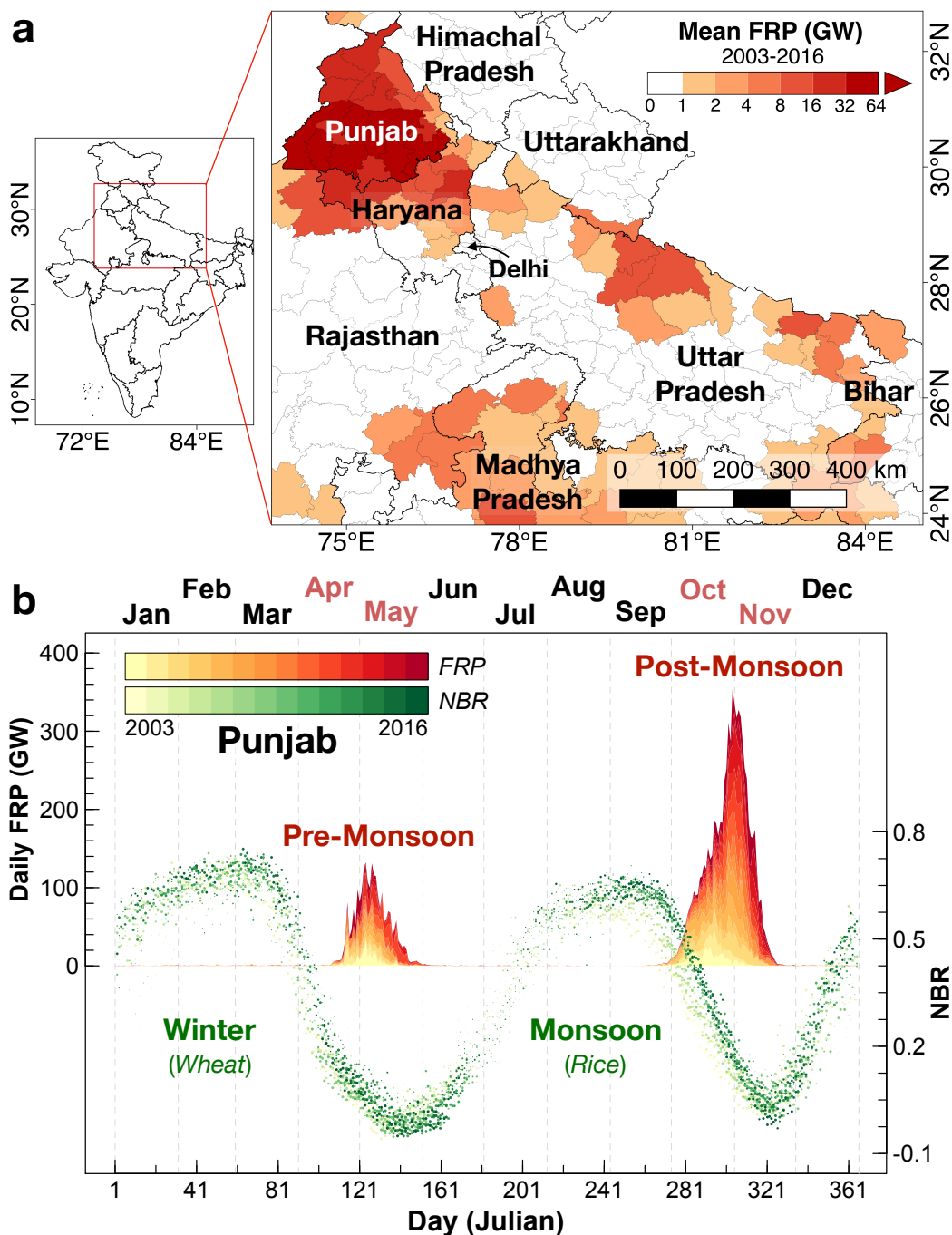
- 359 Amann M, Purohit P, Bhanarkar A D, Bertok I, Borken-Kleefeld J, Cofala J, Heyes C,
360 Kieseewetter G, Klimont Z, Liu J, Majumdar D, Nguyen B, Rafaj P, Rao P S, Sander R,
361 Schöpp W, Srivastava A and Vardhan B H 2017 Managing future air quality in megacities:
362 A case study for Delhi *Atmos. Environ.* **161** 99–111 Online:
363 <https://doi.org/10.1016/j.atmosenv.2017.04.041>
- 364 Asner G P and Lobell D B 2000 A Biogeophysical Approach for Automated SWIR Unmixing of
365 Soils and Vegetation *Remote Sens. Environ.* **74** 99–112 Online:
366 [https://doi.org/10.1016/S0034-4257\(00\)00126-7](https://doi.org/10.1016/S0034-4257(00)00126-7)
- 367 Asoka A, Gleeson T, Wada Y and Mishra V 2017 Relative contribution of monsoon precipitation

- 368 and pumping to changes in groundwater storage in India *Nat. Geosci.* **10** 109–17 Online:
369 <https://doi.org/10.1038/ngeo2869>
- 370 Avery T E and Berlin G L 1992 *Fundamentals of remote sensing and airphoto interpretation*
371 (New York, NY: Macmillan Publishing Company)
- 372 Azzari G, Jain M and Lobell D B 2017 Towards fine resolution global maps of crop yields:
373 Testing multiple methods and satellites in three countries *Remote Sens. Environ.* **202** 129–
374 41 Online: <http://dx.doi.org/10.1016/j.rse.2017.04.014>
- 375 Badarinath K V S, Kiran Chand T R and Krishna Prasad V 2006 Agriculture crop residue
376 burning in the Indo-Gangetic Plains - A study using IRS-P6 AWiFS satellite data *Curr. Sci.*
377 **91** 1085–9
- 378 Balwinder-Singh, Humphreys E, Gaydon D S and Eberbach P L 2016 Evaluation of the effects
379 of mulch on optimum sowing date and irrigation management of zero till wheat in central
380 Punjab, India using APSIM *F. Crop. Res.* **197** 83–96 Online:
381 <http://dx.doi.org/10.1016/j.fcr.2016.08.016>
- 382 Bikkina S, Andersson A, Kirillova E N, Holmstrand H, Tiwari S, Srivastava A K, Bisht D S and
383 Gustafsson Ö 2019 Air quality in megacity Delhi affected by countryside biomass burning
384 *Nat. Sustain.* Online: <https://doi.org/10.1038/s41893-019-0219-0>
- 385 Chen D, Huang J and Jackson T J 2005 Vegetation water content estimation for corn and
386 soybeans using spectral indices derived from MODIS near- and short-wave infrared bands
387 *Remote Sens. Environ.* **98** 225–36 Online: <https://doi.org/10.1016/j.rse.2005.07.008>
- 388 Choudhury S, Rajpal H, Saraf A K and Panda S 2007 Mapping and forecasting of North Indian
389 winter fog: an application of spatial technologies *Int. J. Remote Sens.* **28** 3649–63 Online:
390 <https://doi.org/10.1080/01431160600993470>
- 391 Cusworth D H, Mickley L J, Sulprizio M P, Liu T, Marlier M E, DeFries R S, Guttikunda S K
392 and Gupta P 2018 Quantifying the influence of agricultural fires in northwest India on urban
393 air pollution in Delhi, India *Environ. Res. Lett.* **13** 044018 Online:
394 <https://doi.org/10.1088/1748-9326/aab303>
- 395 Dey S 2018 On the theoretical aspects of improved fog detection and prediction in India *Atmos.*
396 *Res.* **202** 77–80 Online: <https://doi.org/10.1016/j.atmosres.2017.11.018>
- 397 Dreze J and Khera R 2015 Understanding Leakages in the Public Distribution System *Econ.*
398 *Polit. Wkly.* **L** 39–42
- 399 Eva H and Lambin E F 1998 Burnt area mapping in Central Africa using ATSR data *Int. J.*
400 *Remote Sens.* **18** 3473–97 Online: <https://doi.org/10.1080/014311698213768>
- 401 Gautam R and Singh M K 2018 Urban Heat Island Over Delhi Punches Holes in Widespread
402 Fog in the Indo-Gangetic Plains *Geophys. Res. Lett.* **45** Online:
403 <https://doi.org/10.1002/2017GL076794>
- 404 Ghude S D, Bhat G S, Prabhakaran T, Jenamani R K, Chate D M, Safai P D, Karipot A K,
405 Konwar M, Pithani P, Sinha V, Rao P S P, Dixit S A, Tiwari S, Todekar K, Varpe S,
406 Srivastava A K, Bisht D S, Murugavel P, Ali K, Mina U, Dharua M, Jaya Rao Y,
407 Padmakumari B, Hazra A, Nigam N, Shende U, Lal D M, Chandra B P, Mishra A K,
408 Kumar A, Hakkim H, Pawar H, Acharja P, Kulkarni R, Subharthi C, Balaji B, Varghese M,
409 Bera S and Rajeevan M 2017 Winter fog experiment over the Indo-Gangetic plains of India

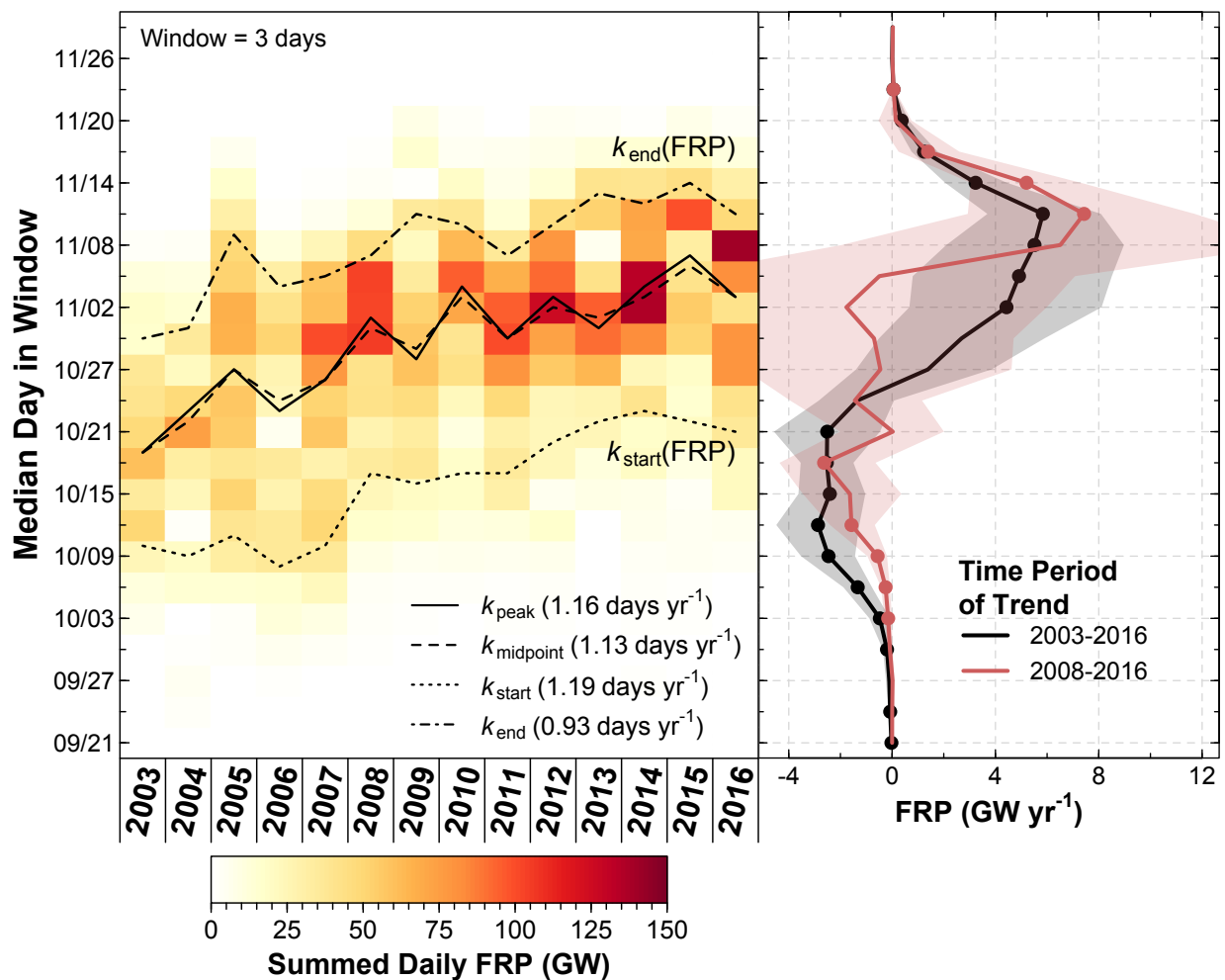
- 410 *Curr. Sci.* **112** 767–84 Online: <https://doi.org/10.18520/cs/v112/i04/767-784>
- 411 Giglio L, Schroeder W and Justice C O 2016 The collection 6 MODIS active fire detection
412 algorithm and fire products *Remote Sens. Environ.* **178** 31–41 Online:
413 <https://doi.org/10.1016/j.rse.2016.02.054>
- 414 Gorelick N, Hancher M, Dixon M, Ilyushchenko S, Thau D and Moore R 2017 Google Earth
415 Engine: Planetary-scale geospatial analysis for everyone *Remote Sens. Environ.* **202** 18–27
416 Online: <https://doi.org/10.1016/j.rse.2017.06.031>
- 417 Humphreys E, Kukal S S, Christen E W, Hira G S, Balwinder-Singh, Sudhir-Yadav and Sharma
418 R K 2010 Halting the groundwater decline in north-west India-which crop technologies will
419 be winners? *Adv. Agron.* **109** 155–217 Online: [https://doi.org/10.1016/B978-0-12-385040-](https://doi.org/10.1016/B978-0-12-385040-9.00005-0)
420 [9.00005-0](https://doi.org/10.1016/B978-0-12-385040-9.00005-0)
- 421 Jain M, Mondal P, DeFries R S, Small C and Galford G L 2013 Mapping cropping intensity of
422 smallholder farms: A comparison of methods using multiple sensors *Remote Sens. Environ.*
423 **134** 210–23 Online: <http://dx.doi.org/10.1016/j.rse.2013.02.029>
- 424 Jain M, Mondal P, Galford G, Fiske G and DeFries R 2017 An Automated Approach to Map
425 Winter Cropped Area of Smallholder Farms across Large Scales Using MODIS Imagery
426 *Remote Sens.* **9** 566 Online: <http://www.mdpi.com/2072-4292/9/6/566>
- 427 Jethva H, Chand D, Torres O, Gupta P, Lyapustin A and Patadia F 2018 Agricultural Burning
428 and Air Quality over Northern India: A Synergistic Analysis using NASA’s A-train Satellite
429 Data and Ground Measurements *Aerosol Air Qual. Res.* **18** 1756–73 Online:
430 <http://doi.org/10.4209/aaqr.2017.12.0583>
- 431 Justice C O, Townshend J R G, Holben B N and Tucker C J 1985 Analysis of the phenology of
432 global vegetation using meteorological satellite data *Int. J. Remote Sens.* **6** 1271–318
433 Online: <https://doi.org/10.1080/01431168508948281>
- 434 Kaskaoutis D G, Kumar S, Sharma D, Singh R P, Kharol S K, Sharma M, Singh A K, Singh S,
435 Singh A and Singh D 2014 Effects of crop residue burning on aerosol properties, plume
436 characteristics, and long-range transport over northern India *J. Geophys. Res. Atmos.* **119**
437 5424–44 Online: <https://doi.org/10.1002/2013JD021357>
- 438 Key C H and Benson N C 2006 *Landscape Assessment (LA)*. In: Lutes, Duncan C.; Keane,
439 Robert E.; Caratti, John F.; Key, Carl H.; Benson, Nathan C.; Sutherland, Steve; Gangi,
440 Larry J. 2006. *FIREMON: Fire effects monitoring and inventory system* Online:
441 https://www.fs.fed.us/rm/pubs/rmrs_gtr164/rmrs_gtr164_13_land_assess.pdf
- 442 Kumar P, Kumar S and Joshi L 2015 *Socioeconomic and Environmental Implications of*
443 *Agricultural Residue Burning: A Case Study of Punjab, India* Online:
444 <https://doi.org/10.1007/978-81-322-2014-5>
- 445 Liu T, Marlier M E, DeFries R S, Westervelt D M, Xia K R, Fiore A M, Mickley L J, Cusworth
446 D H and Milly G 2018 Seasonal impact of regional outdoor biomass burning on air
447 pollution in three Indian cities: Delhi, Bengaluru, and Pune *Atmos. Environ.* **172** 83–92
448 Online: <https://doi.org/10.1016/j.atmosenv.2017.10.024>
- 449 Liu T, Marlier M E, Karambelas A, Jain M, Singh S, Singh M K, Gautam R and DeFries R S
450 2019 Missing emissions from post-monsoon agricultural fires in northwestern India:
451 regional limitations of MODIS burned area and active fire products *Environ. Res. Commun.*
452 **1** 011007 Online: <https://doi.org/10.1088/2515-7620/ab056c>

- 453 Lobell D B, Ortiz-Monasterio J I, Sibley A M and Sohu V S 2013 Satellite detection of earlier
454 wheat sowing in India and implications for yield trends *Agric. Syst.* **115** 137–43 Online:
455 <http://dx.doi.org/10.1016/j.agsy.2012.09.003>
- 456 Lobell D B, Sibley A and Ivan Ortiz-Monasterio J 2012 Extreme heat effects on wheat
457 senescence in India *Nat. Clim. Chang.* **2** 186–9 Online:
458 <http://dx.doi.org/10.1038/nclimate1356>
- 459 Mondal P, Jain M, DeFries R S, Galford G L and Small C 2015 Sensitivity of crop cover to
460 climate variability: Insights from two Indian agro-ecoregions *J. Environ. Manage.* **148** 21–
461 30 Online: <http://dx.doi.org/10.1016/j.jenvman.2014.02.026>
- 462 Mondal P, Jain M, Robertson A W, Galford G L, Small C and DeFries R S 2014 Winter crop
463 sensitivity to inter-annual climate variability in central India *Clim. Change* **126** 61–76
- 464 Mukherjee J, Das D K, Sehgal V K, Vashisth A, Singh R and Barari S K 2014 South west
465 monsoon and food grain production of India *J. Agric. Phys.* **14** 73–9
- 466 NSSO 2014 *Key Indicators of Situation of Agricultural Households in India* Online:
467 http://mospi.nic.in/sites/default/files/publication_reports/KI_70_33_19dec14.pdf
- 468 Platnick S, King M D, Ackerman S A, Menzel W P, Baum B A, Riédi J C and Frey R A 2003
469 The MODIS cloud products: Algorithms and examples from Terra *IEEE Trans. Geosci.*
470 *Remote Sens.* **41** 459–73 Online: <https://doi.org/10.1109/TGRS.2002.808301>
- 471 Ramanathan V, Chung C, Kim D, Bettge T, Buja L, Kiehl J T, Washington W M, Fu Q, Sikka D
472 R and Wild M 2005 Atmospheric brown clouds: Impacts on South Asian climate and
473 hydrological cycle *Proc. Natl. Acad. Sci.* **102** 5326–33 Online:
474 <https://doi.org/10.1073/pnas.0500656102>
- 475 Reddy D N, Reddy A A and Bantilan M C S 2014 The impact of Mahatma Gandhi National
476 Rural Employment Guarantee Act (MGNREGA) on rural labor markets and agriculture
477 *India Rev.* **13** 251–73
- 478 Roy D P, Giglio L, Kendall J D and Justice C O 1999 Multi-temporal active-fire based burn scar
479 detection algorithm *Int. J. Remote Sens.* **20** 1031–8 Online:
480 <https://doi.org/10.1080/014311699213073>
- 481 Saraf A, Bora A, Das J, Rawat V, Sharma K and Jain S K 2010 Winter fog over the Indo-
482 Gangetic Plains: Mapping and modelling using remote sensing and GIS *Nat. Hazards* **52**
483 199–220 Online: <https://doi.org/10.1007/s11069-010-9660-0>
- 484 Sarkar S, Singh R P and Chauhan A 2018 Crop Residue Burning in Northern India: Increasing
485 Threat to Greater India *J. Geophys. Res. Atmos.* **123** 6920–34
- 486 Sidhu H S, Singh M, Yadvinder S, Blackwell J, Lohan S K, Humphreys E, Jat M L, Singh V and
487 Singh S 2015 Development and evaluation of the Turbo Happy Seeder for sowing wheat
488 into heavy rice residues in NW India *F. Crop. Res.* **184** 201–12 Online:
489 <https://doi.org/10.1016/j.fcr.2015.07.025>
- 490 Singh K 2009 Act to Save Groundwater in Punjab: Its Impact on Water Table, Electricity
491 Subsidy and Environment *Agric. Econ. Res. Rev.* **22** 365–386
- 492 Sinha B, Singh Sangwan K, Maurya Y, Kumar V, Sarkar C, Chandra B P and Sinha V 2015
493 Assessment of crop yield losses in Punjab and Haryana using 2 years of continuous in situ
494 ozone measurements *Atmos. Chem. Phys.* **15** 9555–76

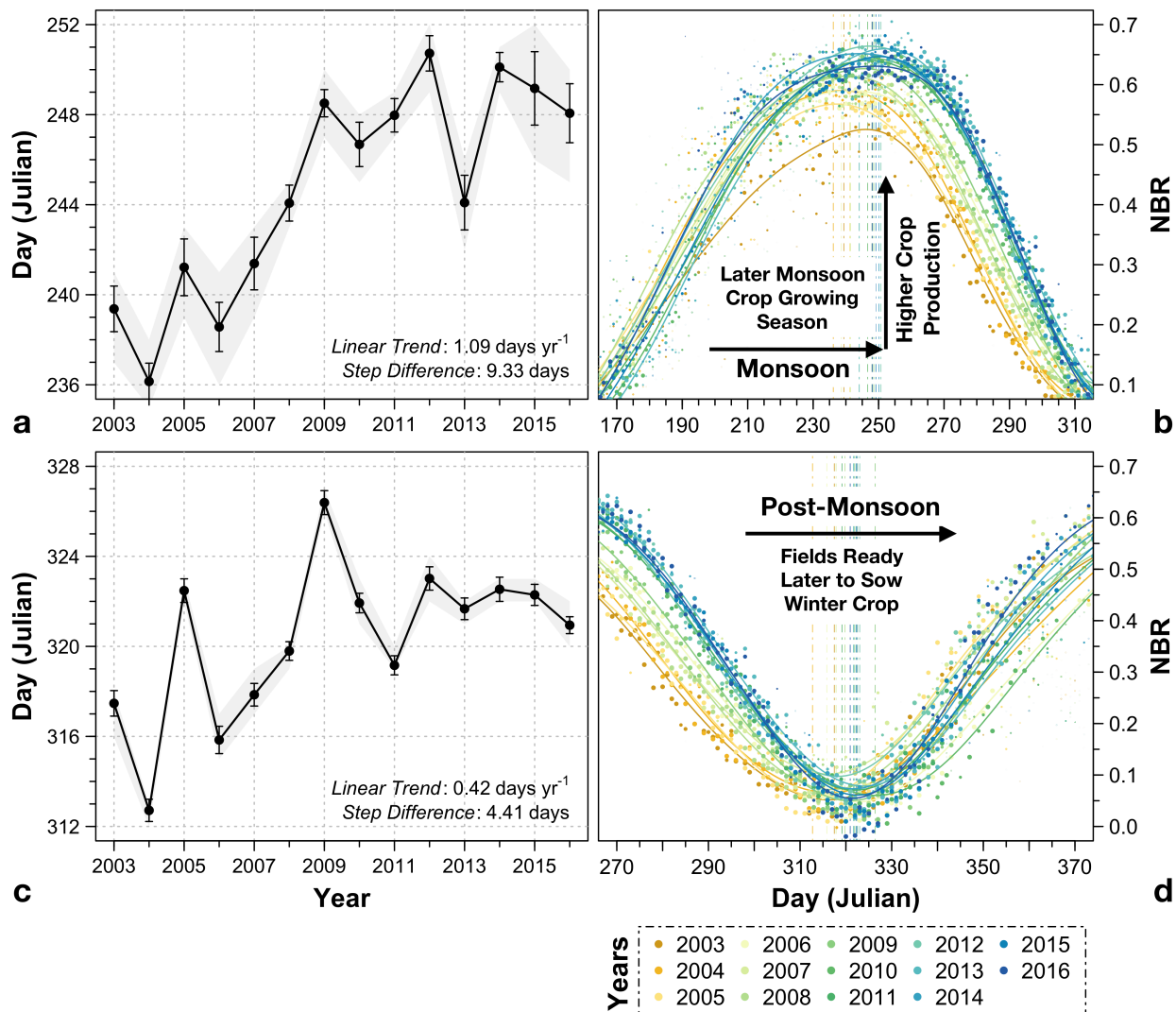
- 495 Swaminathan M 2000 *Weakening Welfare: The Public Distribution of Food in India* (LeftWord
496 Books)
- 497 Tallis H, Polasky S, Shyamsundar P, Springer N, Ahuja V, Cummins J, Datta I, Dixon J, Gerard
498 B, Ginn W, Gupta R, Jadhav A, Jat M, Keil A, Krishnapriya P, Ladha J, Nandrajog S, Paul
499 S, Lopez Ridaura S, Ritter A, Sidhu H, Skiba N and Somanathan R 2017 *The Evergreen
500 Revolution: Six Ways to empower India's no-burn agricultural future* Online:
501 <https://www.nature.org/science-in-action/the-evergreen-revolution.pdf>
- 502 Thumaty K C, Rodda S R, Singhal J, Gopalakrishnan R, Jha C S, Parsi G D and Dadhwal V K
503 2015 Spatio-temporal characterization of agriculture residue burning in Punjab and
504 Haryana, India, using MODIS and Suomi NPP VIIRS data *Curr. Sci.* **109** 1850–5 Online:
505 <https://doi.org/10.18520/v109/i10/1850-1855>
- 506 Tripathi A, Mishra A K and Verma G 2016 Impact of Preservation of Subsoil Water Act on
507 Groundwater Depletion: The Case of Punjab, India *Environ. Manage.* **58** 48–59
- 508 Yengoh G T, Dent D, Olsson L, Tengberg A E and Tucker C J 2015 *Use of the Normalized
509 Difference Vegetation Index (NDVI) to Assess Land Degradation at Multiple Scales:
510 Current Status, Future Trends, and Practical Considerations* (Springer International
511 Publishing)
- 512 Zhang X, Kondragunta S and Roy D P 2014 Interannual variation in biomass burning and fire
513 seasonality derived from geostationary satellite data across the contiguous United States
514 from 1995 to 2011 *J. Geophys. Res. Biogeosciences* **119** 1147–62 Online:
515 <https://doi.org/10.1002/2013JG002518>
- 516 Zhao H, Yang Z, Di L, Li L and Zhu H 2009 Crop phenology date estimation based on NDVI
517 derived from the reconstructed MODIS daily surface reflectance data 2009 *17th Int. Conf.
518 Geoinformatics* 3–8



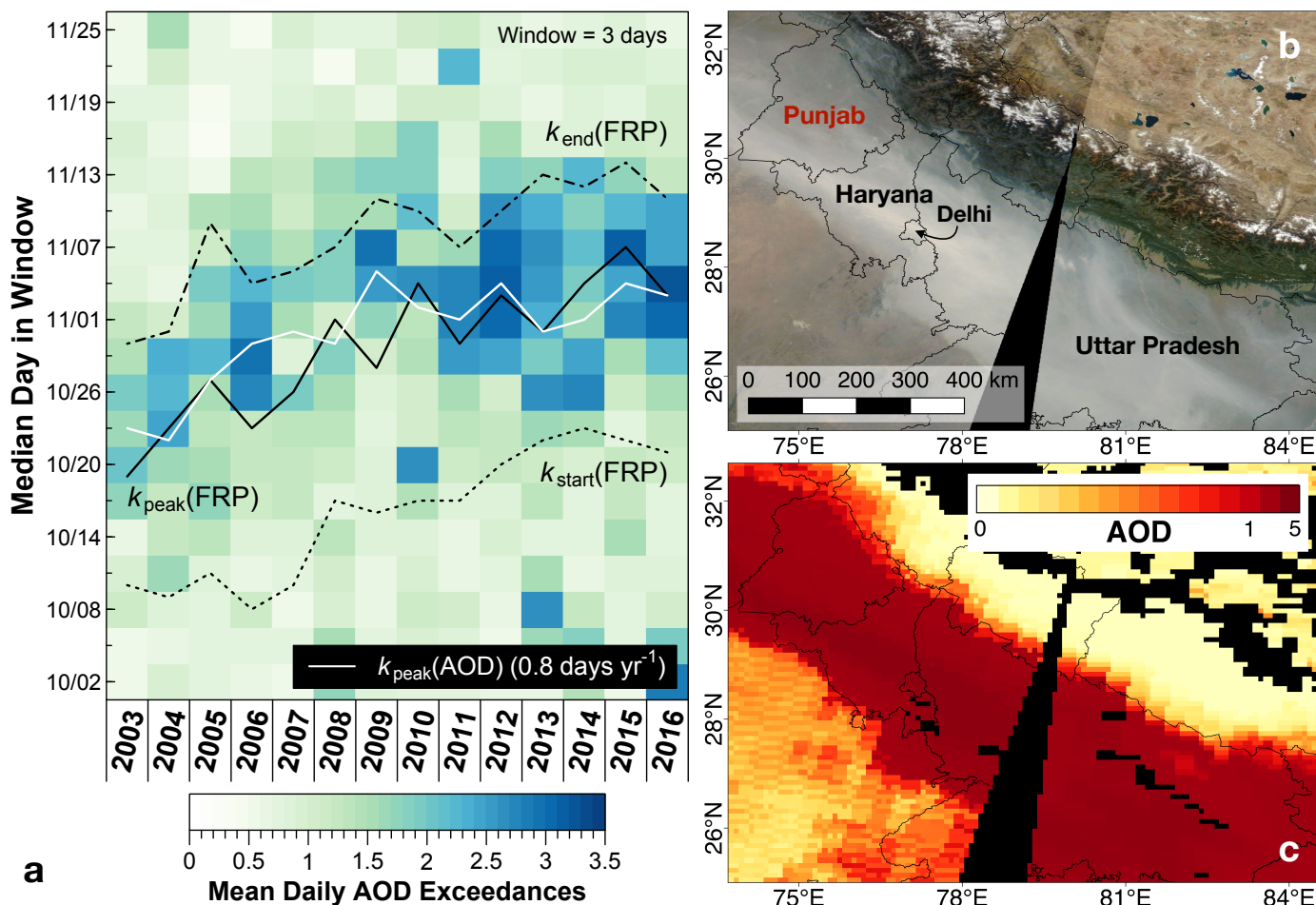
519
 520 **Figure 1. Cycles of fire activity and vegetation greenness in Punjab, India.** District-level
 521 maps of (a) the Indo-Gangetic Plain (IGP) overlaid with annual agricultural MODIS Aqua +
 522 Terra Fire Radiative Power (GW), averaged over 2003-2016. (b) Daily FRP (left axis) and
 523 median Normalized Burn Ratio (NBR; right axis) in Punjab. FRP values are stacked with earlier
 524 years on the bottom. The double-crop cycle indicated by NBR, a proxy for greenness, is
 525 predominantly a rice-wheat rotation. Pre-monsoon fires occur from April to May after the winter
 526 wheat growing season, and post-monsoon fires occur from October to November after the
 527 monsoon rice growing season.



528
 529 **Figure 2. Temporal shifts in post-monsoon fires in Punjab from 2003-2016.** (left) Each block
 530 represents the 3-day summed Fire Radiative Power (FRP). Dashed and solid lines represent the
 531 timing of the start, peak, midpoint, and end of the post-monsoon burning season, based on daily
 532 observations of FRP. Text inset in the left panel shows the linear trends in the $k_{start}(FRP)$,
 533 $k_{midpoint}(FRP)$, $k_{peak}(FRP)$, and $k_{end}(FRP)$; all trends shown are statistically significant at
 534 the 95% confidence level. (right) Trends in summed FRP ($GW\ yr^{-1}$) for each 3-day block
 535 window from September 20 to November 30 for the 2003-2016 (black line) and 2008-2016 time
 536 periods (red line). The shaded envelopes denote the 95% confidence interval, and dots represent
 537 statistically significant increases or decreases in 3-day block FRP.



538
 539 **Figure 3. Trends in monsoon peak greenness and post-monsoon trough greenness in**
 540 **Punjab from 2003-2016.** Bootstrapped mean maximum NBR during the (a) monsoon crop
 541 growing season and (c) post-monsoon harvest season, from 2003-2016. Error bars show one σ
 542 uncertainty, and shaded gray envelopes denote the 95% confidence interval. Text inset shows the
 543 bootstrapped linear trend in the timing of (a) maximum monsoon greenness and (c) minimum
 544 post-monsoon greenness from 2003-2016 and mean step difference between the 2003-2007 and
 545 2008-2016 time periods. Daily median NBR during the (b) monsoon crop growing season and
 546 (d) post-monsoon harvest season, with lines showing the weighted parabola smoothing. Different
 547 colors denote different years. The bootstrapped mean day of (b) maximum monsoon greenness
 548 and (d) minimum post-monsoon greenness of each year is shown by vertical dashed-dot lines.



550 **Figure 4. Trend in the timing of peak post-monsoon AOD over the western Indo-Gangetic**
 551 **Plain from 2003-2016.** (a) Each block represents the 3-day average of regional aerosol optical
 552 depth (AOD) exceedances from the MODIS/Terra Deep Blue retrieval algorithm over Punjab,
 553 Haryana, Delhi, and western Uttar Pradesh. Here exceedances are defined as the spatially
 554 averaged AOD increments above the mean AOD + 1σ for each season and pixel. Dashed lines
 555 represent the timing of the start, peak, and end of the post-monsoon burning season, based on
 556 daily FRP (same as in Figure 2). Text shows the linear trend in the $k_{peak}(AOD)$, statistically
 557 significant at the 95% confidence level. Example of thick haze over the western IGP on
 558 November 6, 2016, as observed by MODIS/Terra, shown as (b) true color and (c) Deep Blue
 559 AOD (NASA/Worldview; <https://worldview.earthdata.nasa.gov/>). The colorbar in (c) is
 560 logarithmic.